

Highlights

Generalization of composite dynamics for the lattice Boltzmann method

Julius Weinmiller, Benjamin Kellers, Martin P. Lautenschlaeger, Arnulf Latz, Timo Danner

- A generalized framework for composite dynamics is proposed for the lattice Boltzmann method, enabling systematic combination of collision operators.
- This framework gives insight into force inclusion and analysis of existing composite dynamics.
- It allows for straightforward creation of new composite dynamics to model complex phenomena.

Generalization of composite dynamics for the lattice Boltzmann method

Julius Weinmiller^{a,b}, Benjamin Kellers^{a,b}, Martin P. Lautenschlaeger^{a,b,c}, Arnulf Latz^{a,b,d}, Timo Danner^{a,b}

^a*Institute of Engineering Thermodynamics, German Aerospace Center (DLR), Ulm, Germany*

^b*Helmholtz Institute Ulm for Electrochemical Energy Storage (HIU), Ulm, Germany*

^c*SDU Mechatronics, Department of Mechanical and Electrical Engineering, University of Southern Denmark (SDU), Sønderborg, Denmark*

^d*Institute of Electrochemistry, Ulm University, Ulm, Germany*

Abstract

A generalized composite dynamics framework is presented for the lattice Boltzmann method. It leverages synergies of various simple collision operators to model intertwined physical processes, capturing complex behavior. The framework is validated by recovering partial bounceback fluid flow methods. Systematic derivation in our framework provides mathematical justification for the incorporation of forces, addressing a gap in the literature. The versatility of this framework is demonstrated by analyzing a robin boundary condition. Moreover, two new dynamics are proposed using our generalized framework, namely the partial robin boundary condition, and transfer partial bounceback. The generalized composite dynamics framework opens innovative possibilities for simulating complex phenomena using lattice Boltzmann methods, demonstrated here with sub-grid wall reactions and reactive porous media.

Keywords: Lattice Boltzmann, composite dynamics, grayscale methods

2000 MSC: 76S05, 76P05, 76M50, 76M28, 80A32, 80M40, 80A20

1. Introduction

Complex physical phenomena are a combination of multiple processes collectively creating intricate behavior. Often, the effects of these processes are convoluted and cannot be separated easily. To understand and simulate such phenomena, computational approaches should ideally depict the underlying complex processes.

The lattice Boltzmann method (LBM) is a powerful computational technique for simulating transport

phenomena and related processes, known for its inherent simplicity and versatility [1, 2]. It represents microscopic particles using a discrete-velocity distribution function – the so-called population – in a discretized phase space, using a lattice and grid, for the velocity and space, respectively. The macroscopic properties and behavior emerge through the collision and streaming of populations. However, only a single dynamic – via the collision – can be applied to a grid location. A dynamic describes a specific behav-

ior. Using only simple dynamics therefore limits the applicability of LBM.

Composite dynamics are a progression to mitigate these limitations. They are a combination of simple dynamics, that have synergistic effects from which intricate behavior emerge. In literature, they have been mostly discussed in the context of solid-fluid composites, often called partial bounceback [3, 4, 5, 6, 7, 8, 9, 10, 11], but also used in solid-solid [12, 13, 14, 15] and other interactions [16, 17, 18, 19]. LBM literature also contains composite dynamics which are not treated as such, e.g. reactive boundary conditions [20, 21, 22, 23]. Applications are, e.g. semi-permeable materials [11, 9, 6, 24], single- and multi-phase flow within porous media [16, 17, 25, 26, 27, 10, 28, 29, 30], material dissolution [31, 32, 33, 34], and (sharp) interface handling [12, 14, 4, 18]. While not a new concept, composite dynamics have been developed with a focus on individual challenges without an unifying framework.

This paper is motivated by the need for a mathematically sound basis for composite dynamics. Existing composite dynamics typically only use and act upon the total population. To the best of the authors' knowledge, the work by Yu et al. [10] is the exception, where the dynamics act only on population parts. This approach is also used here to reinterpret solid-fluid composite dynamics and generalize composite dynamics into a unified framework.

In the following, we present a novel generalized composite dynamics (GCD) framework for LBM.

This framework provides a systematic approach to combine various simple dynamics. Hence, it opens new avenues for simulating and comprehending complex physical phenomena.

Establishing a systematic framework allows for a top-down analysis of existing methods, as well as a bottom-up creation of novel ones. This makes the framework versatile and applicable to many different fields. It is a significant step to relate complex macroscopic behavior to microscopic collision operators.

In this paper, we first present the GCD framework in Section 2.1. Then the dynamics used in this paper are shown in Section 2.2. To substantiate the framework, we will show how existing methods can be interpreted, and new ones created in Section 3. We cover semi-permeable flow methods via partial bounceback with and without forces, and a novel analysis and rewriting of the robin boundary conditions for the existing methods. Newly derived dynamics include partial robin boundary conditions and reactive porous advection-diffusion.

2. Methodology

In this section, we introduce the generalized composite dynamics framework, which provides insight into analyzing existing dynamics and combining dynamics to generate new behavior. Additionally, the base dynamics used in this paper are defined.

2.1. Generalized composite dynamics

In LBM, advection and diffusion of the discrete-velocity distribution function f_i emerges through local

collision and subsequent streaming of f_i . The local collision is governed via the collision operator Ω , which acts on f_i . Essentially, Ω is a rule or algorithm to define the local behavior of f_i , from which the relevant physics emerge. The Bhatnagar, Gross, and Krook (BGK) collision operator [35] and the bounce-back (BB) collision operator [36, 37] are commonly used to model fluid flow and no-slip walls, respectively, and are hereafter denoted as Ω^{BGK} and Ω^{BB} .

The GCD framework assumes that the local complex behavior can be described as a sum of simpler behaviors. In LBM that means that the local collision is composed of a set of N dynamics. The n^{th} dynamic acts on population part f_i^n . The total population is the sum of the population parts $f_i = \sum_n f_i^n$. This allows for the following straightforward and general collision rule and streaming step

$$f_i^*(\mathbf{x}, t) = f_i + \sum_n [\Omega^n(f_i^n) + S_i^n] \Delta t, \quad (1)$$

$$f_i(\mathbf{x} + \mathbf{c}_i \Delta t, t + \Delta t) = f_i^*(\mathbf{x}, t). \quad (2)$$

Here, \mathbf{x} and t denote the location in discretized space and time. The star symbol $*$ indicates a post-collision state, Δt is the time step, and \mathbf{c}_i the discrete velocity along the i^{th} lattice direction. The shorthand notation $f_i = f_i(\mathbf{x}, t)$ is used throughout this paper. The superscript n denotes the parts of the population f_i^n that undergo the corresponding dynamics Ω^n or are affected by a further source term S_i^n .

The population is decomposed into the population parts via

$$f_i^n := \eta_i^n(\mathbf{x}, t) f_i, \quad \sum_n \eta_i^n(\mathbf{x}, t) = 1, \quad (3)$$

where $\eta_i^n(\mathbf{x}, t) \in [0, 1]$ is the composite fraction. It quantifies the portion of the total population that is affected by Ω^n .

The corresponding population part n -specific mass density ρ^n and momentum density $(\rho \mathbf{u})^n$ are defined as

$$\rho^n := \sum_i f_i^n + \frac{\Delta t}{2} \sum_i [\Omega^n(f_i^n) + S_i^n], \quad (4)$$

$$(\rho \mathbf{u})^n := \sum_i f_i^n \mathbf{c}_i + \frac{\Delta t}{2} \sum_i [\Omega^n(f_i^n) + S_i^n] \mathbf{c}_i, \quad (5)$$

with n -specific velocity \mathbf{u}^n derived from its momentum $\rho^n \mathbf{u}^n = (\rho \mathbf{u})^n$.

The macroscopic total density, ρ^{tot} , and total momentum, $(\rho \mathbf{u})^{\text{tot}}$, are recombined from these n -specific properties via

$$\rho^{\text{tot}} = \sum_n \rho^n, \quad (\rho \mathbf{u})^{\text{tot}} = \sum_n (\rho \mathbf{u})^n, \quad (6)$$

with $\rho^{\text{tot}} \mathbf{u}^{\text{tot}} = (\rho \mathbf{u})^{\text{tot}}$.

A density source $\Delta \rho^n$ emerges through the second sum in Eq. (4). Usually, the collision term for fluid flow is density conserving, i.e. $\sum_i \Omega^n(f_i) = 0$, and only S_i^n contributes. The total density source is $\Delta \rho^{\text{tot}} = \sum_n \Delta \rho^n$.

A momentum density source from a force density $\Delta(\rho \mathbf{u})^n = \mathbf{K}^n \Delta t$, emerges from the second sum in Eq. (5). This is either achieved directly via the source term S_i^n , or indirectly by a non-conserving collision operator Ω^n , or both. The total force density $\mathbf{K}^{\text{tot}} = \sum_n \mathbf{K}^n$ is used to model macroscopic phenomena.

So far, neither Ω^n nor S_i^n have been defined to keep the formulation as general as possible. However, there are several notes that should be taken into consideration.

For Ω^n , most LBM collision operators may be used. Since the GCD framework in its current form does not modify the streaming step, methods depending on that are not compatible yet. For simplicity, this paper focuses solely on purely local collision operators.

An external force density \mathbf{K}^{ext} corresponding to an acceleration \mathbf{a}^{ext} is given by $\mathbf{K}^{\text{ext}} = \rho \mathbf{a}^{\text{ext}}$. From a physical perspective, the \mathbf{a}^{ext} acts on all composite parts equally. The force density then emerges based on the density being moved, e.g. $\mathbf{K}^n = \rho^n \Delta \mathbf{u}^n / \Delta t$, where $\Delta \mathbf{u}^n / \Delta t = \mathbf{a}^{\text{ext}}$ for a fluid.

An external acceleration applied to parts with a prescribed velocity, e.g. a no-slip wall $n = \text{BB}$, induces no momentum change and thus no force. Therefore, $\sum_i (\Omega_i^{\text{BB}} + S_i^{\text{BB}}) \mathbf{c}_i = \mathbf{K}^{\text{BB}} = 0$. This means that externally applied forces may differ from the emergent total force, i.e. $\mathbf{K}^{\text{tot}} \neq \mathbf{K}^{\text{ext}}$.

A general force description is therefore non-trivial. However, for specific cases, the GCD framework allows for important insights that may be missed otherwise.

This concludes the presentation of the GCD framework. The remainder of this paper is used to demonstrate various applications. This is performed in several steps starting with simple well-known concepts to novel and complex examples. Due to the generality of the GCD framework introduced above, any further discussion requires a specific multi-dynamic example. The dynamics used are introduced next.

2.2. Common collision operators

In this section, some of the commonly seen collision operators in literature are reiterated: BGK dynamics with the weakly compressible equilibrium distribution, bounceback (BB), non-equilibrium bounceback (NEBB), equilibrium scheme (ES), anti-bounceback (ABB), and robin boundary condition (RBC). In this paper, they are either used as base dynamics to create composite dynamics, or are rewritten into such dynamics.

BGK dynamics. This is the simplest method to simulate fluid flow, and hence one of the most popular

$$\Omega^{\text{BGK}}(f_i^n) = -\frac{1}{\tau} (f_i^n - f_i^{\text{eq}^n}). \quad (7)$$

Here, the relaxation time τ defined from the non-dimensional kinematic viscosity $\nu = c_s^2(\tau - 1/2)$, with c_s being the lattice speed of sound. In this paper, only this fluid flow dynamics will be used to showcase the generalized composite dynamics. More complex methods such as the two-relaxation time, multi-relaxation time dynamics, and entropic collision can be utilized as well.

To simulate advection-diffusion, the same BGK dynamics can be used. However, velocities in the equilibrium distribution are imposed and not derived from its population. They are either set to constant values or taken from an external flow solution. It is common to solve the flow simulation in LBM separately, using the same time and spatial resolution, as a coupled simulation.

For LBM, the fluid flow behavior simulated is defined by the equilibrium function used, e.g. weakly

compressible, linear or incompressible fluids [2]. The weakly compressible equilibrium function commonly used in the dynamics above is given as

$$f_i^{\text{eq}n}(\rho^n, \mathbf{u}^n) = w_i \rho^n \left(1 + \frac{c_{i\alpha} u_\alpha^n}{c_s^2} + \frac{u_\alpha^n u_\beta^n (c_{i\alpha} c_{i\beta} - c_s^2 \delta_{\alpha\beta})}{2c_s^4} \right), \quad (8)$$

where $\{w_i\}$ is the lattice weight set, derived from the discretized Boltzmann distribution. The vectors \mathbf{u} and \mathbf{c}_i are written in index notation, e.g. u_α , using Greek letters as spatial indices. Here, $\delta_{\alpha\beta}$ is the Kronecker delta. The lattice weight set has to fulfill the conservation of mass, momentum and rotational isotropy [2].

Bounceback (BB) dynamics. This is the simplest implementation for no-slip walls, i.e. a velocity Dirichlet boundary condition, with a wall velocity \mathbf{u}_w

$$\Omega^{\text{BB}}(f_i^n) = -f_i^n + f_{\bar{i}}^n + 2w_i \rho_w^n \frac{c_{i\alpha} u_{w\alpha}^n}{c_s^2}. \quad (9)$$

The notation \bar{i} indicates the opposite direction of i , i.e. $\mathbf{c}_{\bar{i}} = -\mathbf{c}_i$, and the subscript w is referring to the properties at the wall. Setting $\mathbf{u}_w = 0$ results in the commonly seen bounceback for static walls.

For advection-diffusion, it is possible to approximate a mass or concentration Neumann boundary condition to a Dirichlet boundary condition based on the bounceback [2]. The resulting boundary condition is

$$\Omega^{\text{BB}}(f_i^n) = -f_i^n + f_{\bar{i}}^n + 2w_i \frac{c_{i\alpha} q_{w\alpha}^n}{c_s^2}, \quad (10)$$

where \mathbf{q}_w is the applied flux of the Neumann boundary condition.

As written here, it is known as the fullway version. For transient processes, there is a numerically more accurate method where the bounceback occurs during streaming, known as the halfway version.

Non-equilibrium bounceback (NEBB) dynamics. Similar to the BB dynamics, this is a velocity Dirichlet boundary condition, but it is implemented differently at the mesoscopic level. While it is numerically more accurate, it is not mass conserving and more complex. The collision operator is as follows

$$\Omega^{\text{NEBB}}(f_i^n) = -f_i^{\text{neq}n} + f_{\bar{i}}^{\text{neq}n}, \quad (11)$$

where $f_i^{\text{neq}} = f_i - f_i^{\text{eq}}$, with the equilibrium distribution function f_i^{eq} as introduced in Eq. (8).

Anti-bounceback (ABB) dynamics. This dynamics [38, 39, 40] is a popular method to describe a density Dirichlet boundary condition in LBM. Its collision operator reads

$$\Omega^{\text{ABB}}(f_i^n) = -f_i^n - f_{\bar{i}}^n + 2w_i \rho_w^n \left(1 + \frac{u_{w\alpha}^n u_{w\beta}^n (c_{i\alpha} c_{i\beta} - c_s^2 \delta_{\alpha\beta})}{2c_s^4} \right). \quad (12)$$

Equilibrium scheme (ES). This simple scheme [41, 42] is a method of describing both density and velocity at a boundary, by setting the populations to the equilibrium $f_i^* = f_i^{\text{eq}}$ (cf. Eq. (8)). Hence, its operator is given by

$$\Omega^{\text{ES}}(f_i^n) = -f_i^n + f_i^{\text{eq}n}. \quad (13)$$

While the method is very stable, it is only accurate to first order [2]. Note that when $\tau = 1$, the BGK collision Eq. (7) is equal to the ES.

From Eqs. (8), (9), (12) and (13), it follows that¹

$$\Omega^{\text{ES}}(f_i^n) = \frac{\Omega^{\text{ABB}}(f_i^n) + \Omega^{\text{BB}}(f_i^n)}{2}. \quad (14)$$

This relation shows that the ES is a composite dynamic consisting of anti-BB and BB with equal proportions, i.e. both equally a density and velocity Dirichlet condition.

Robin boundary condition (RBC). This scheme is a combination of both a density Dirichlet and Neumann BC and is popular to describe reactions and heat flows at walls. It models behavior between zero flux and infinitely fast transfer [20, 21, 22, 23, 43]. It describes the mass flux for density fields, first-order reactions for concentration fields, or convection boundaries for temperature fields, with the relevant macroscopic equation

$$\mathbf{q}_w = k_r (\rho_w^{\text{eq}} - \rho). \quad (15)$$

Here, k_r is the transfer coefficient and ρ_w^{eq} is the equilibrium at the wall.

For a general local first-order equilibrium reaction without velocity [20, 21, 22], our group previously showed that a unified formulation can be derived [23]. Here, we show the scheme found in literature, and its rewritten form as a collision operator

$$f_i^* = \frac{2k_i}{1+k_i} w_i \rho_w^{\text{eq}} + \frac{1-k_i}{1+k_i} f_i, \quad (16)$$

$$\Omega^{\text{RBC}}(f_i^n) = -f_i^n + \frac{2k_i}{1+k_i} w_i \rho_w^{\text{eq}n} + \frac{1-k_i}{1+k_i} f_i^n. \quad (17)$$

The $k_i = c_s^{-2} \gamma k_r \cdot (\mathbf{e}_i \cdot \mathbf{n})$ is the directional transfer rate, \mathbf{n} is the wall normal pointing into the fluid, and

¹For interested readers, in Appendix A we additionally derive the relation $(\Omega^{\text{ABB}}(f_i) - \Omega^{\text{BB}}(f_i))/2 = -f_i^{\text{neq}}$.

$\gamma = \tau/(\tau - 0.5)$ is a diffusion correction term. The different schemes in literature differ slightly in the definition of k_i .

With the GCD and the dynamics presented, the next section will look into the various applications and combinations of the shown methods.

3. Applications of the generalized composite dynamics framework

In the following we present several applications of the generalized composite dynamics framework. First, we present existing partial bounceback methods for semi-permeable flow, where parallels to the GCD can be drawn directly. This is followed by a discussion on force inclusion for partial bounceback methods, and how the GCD framework delivers valuable insights. Afterwards, GCD is applied to analyze a RBC, demonstrating a straightforward way to extend it. Finally, two new applications are introduced, covering reactive membranes and partially reactive walls.

3.1. Partial bounceback methods without force

In this part, it is shown how the GCD framework can be applied to recover the partial bounceback methods (PBB) found in literature [11, 3, 4, 5]. These methods are used to either smooth curved solid-fluid interfaces or simulate flow in unresolved porous media.

First, the PBB methods are looked at without considering forces. The aim here is not to improve

upon these existing methods, whose shortcomings and improvements are discussed elsewhere, see e.g. Ref. [44, 45]. The aim is to consider them from a different perspective and express them in a common framework. For simplicity, $\Delta t = 1$ is used.

The PBB methods are interpreted as a composite dynamic superimposing no-slip walls and fluid flow. With the GCD framework, this is written as

$$f_i^* = f_i + \Omega^{\text{BGK}}(f_i^{\text{BGK}}) + \Omega^{*\text{BB}}(f_i^{*\text{BB}}). \quad (18)$$

The walls are modeled with a variant of bounceback, denoted by $*\text{BB}$. Directly applicable here is the full-way BB (cf. Eq. (9)) and the NEBB (cf. Eq. (11)), which results in methods already existing in literature [11, 4]. Only the BGK collision operator is considered here for the fluid flow.

Within this new framework, the various implementations given in literature can be compared more easily, with similarities and differences highlighted. The GCD reformulation of a few selected methods are detailed in Appendix B.

The macroscopic physical behavior is controlled via the composite fractions. In literature, a bounceback weighting factor is used, often misnomered as solid fraction and depicted with n_s . It is equivalent to $\eta^{*\text{BB}}$. They are related to the permeability k of the effective porous medium simulated, e.g. $\eta^{*\text{BB}} = (\tau - 0.5)/(2k/c_s^2 + (\tau - 0.5))$ [11, 6]. Considering all the $\eta^{*\text{BB}}$ definitions [7, 4] (cf. Appendix B), the wall composite fraction can be generally ex-

pressed as

$$\eta^{*\text{BB}} = \frac{\tau - 0.5}{A/c_s^2 + B(\tau - 0.5)} = \frac{1}{A/v + B}, \quad (19)$$

where A and B are fitting parameters, with usually $A \propto k$ and $B = 1$. For all methods, the relation $\eta^{\text{BGK}} = (1 - \eta^{*\text{BB}})$ holds.

In the following, the BGK collision of the PBB in literature is recovered. A better understanding of that is helpful for when forces are included. It is usually detailed as [11, 6, 4]

$$(1 - n_s)\Omega^{\text{BGK}}(f_i) = -\frac{1 - n_s}{\tau}(f_i - f_i^{\text{eq}}). \quad (20)$$

Knowing that the operator is linear makes this a trivial exercise. Not taking that route, however, does provide insights which aids in the overall understanding.

The following derivation assumes an absence of density sources, forces, and local isotropy. For local isotropy $\eta_i^n = \eta^n$ is uniform in all directions. In absence of density sources, $\rho^{\text{tot}} = \sum_i f_i$ (cf. Eq. (6)), and an absence of forces results in $S_i^n = 0$. The BGK collision operator without forces is density and momentum conserving

$$\sum_i \Omega^{\text{BGK}}(f_i^{\text{BGK}}) = 0 \quad \text{and} \quad \sum_i \Omega^{\text{BGK}}(f_i^{\text{BGK}})\mathbf{c}_i = 0. \quad (21)$$

This results in the BGK-density and -velocity (cf. Eqs. (4) and (5)) of

$$\rho^{\text{BGK}} = \sum_i f_i^{\text{BGK}}, \quad (\rho \mathbf{u})^{\text{BGK}} = \sum_i f_i^{\text{BGK}}\mathbf{c}_i, \quad (22)$$

$$\rho^{\text{BGK}} = \eta^{\text{BGK}}\rho^{\text{tot}}, \quad \mathbf{u}^{\text{BGK}} = \frac{1}{\rho^{\text{tot}}}\sum_i f_i\mathbf{c}_i. \quad (23)$$

Here, the η^{BGK} in the velocity cancels out.

In literature, the conventional non-GCD density and velocity definition for BGK are

$$\rho = \sum_i f_i, \quad \mathbf{v} = \frac{1}{\rho} \sum_i f_i \mathbf{c}_i. \quad (24)$$

The \mathbf{u}^{BGK} coincides with \mathbf{v} . Thus, using Eqs. (23) and (24), the equilibrium distribution (cf. Eq. (8)) can be expressed as

$$f_i^{\text{eqBGK}}(\rho^{\text{BGK}}, \mathbf{u}^{\text{BGK}}) = \eta^{\text{BGK}} f_i^{\text{eq}}(\rho, \mathbf{v}). \quad (25)$$

It is then possible to factor out η^{BGK} from the BGK collision operator, resulting in

$$\Omega^{\text{BGK}}(f_i^{\text{BGK}}) = -\frac{\eta^{\text{BGK}}}{\tau} (f_i - f_i^{\text{eq}}) = \eta^{\text{BGK}} \Omega^{\text{BGK}}(f_i). \quad (26)$$

Finally, expressing η^{BGK} as $1 - n_s$, results in the conventional BGK collision operator for PBB (cf. Eq. (20)).

An important distinction to be made in PBB is regarding the ‘‘macroscopic velocity’’, which is the velocity of the phenomena observed. Here, in the GCD framework, it is the total velocity \mathbf{u}^{tot} (cf. Eq. (6)).

In comparison to the literature, it is straightforward to derive. By definition, both collision operators used are mass conserving (cf. Eq. (21)) and $\sum_i \Omega^{\text{BB}}(f_i^{\text{BB}}) = 0$. Hence $\rho^{\text{tot}} = \sum_i f_i$.

However, for momentum, only the BGK collision operator is conserving (cf. Eq. (21)), with

$$\sum_i \Omega^{\text{BB}}(f_i^{\text{BB}}) \mathbf{c}_i = -2(\rho \mathbf{u})^{\text{BB}}. \quad (27)$$

Hence, $(\rho \mathbf{u})^{\text{tot}} = \sum_i f_i \mathbf{c}_i - (\rho \mathbf{u})^{\text{BB}} = (1 - \eta^{\text{BB}}) (\rho \mathbf{u})^{\text{tot}}$, which is the same as in literature, but systematically derived.

It is important to note that $\Omega^{\text{BGK}}(f_i^{\text{BGK}})$ uses \mathbf{u}^{BGK} , and $\Omega^{*\text{BB}}(f_i^{*\text{BB}})$ uses $\mathbf{u}^{*\text{BB}}$, and in general $\mathbf{u}^n \neq \mathbf{u}^{\text{tot}}$. This distinction is not immediately evident, since Ω^{BB} for stationary walls is not velocity dependent, and \mathbf{u}^{BGK} coincides with the conventional fluid velocity definition \mathbf{v} .

This distinction becomes important when $\mathbf{u}^{*\text{BB}}$ is set, or $\Omega^{*\text{BB}}$ is a function of velocity, e.g. when simulating moving walls, or suspended particles. For instance in Ref. [4] the authors correctly noted the usage of solid velocity in the NEBB, albeit with limited explanation.

3.2. Forced partial bounceback methods

In this part, the GCD framework is used to include forces to the partial bounceback methods discussed in the previous section. Forces allows for simulating gravity driven or multiphase flow. This further highlights the importance to distinguish between the various velocities. Here again, $\Delta t = 1$.

Two popular LBM schemes are investigated: Guo forcing [46] and Shan-Chen (SC) forcing [47]. In Guo forcing, momentum is redistributed via S_i^n (cf. Eq. (1)), whereas in SC forcing the force effects are incorporated solely through Ω^n . It can, however, be rewritten as a sole source term as well [45].

When using SC forcing, the force effects emerge by breaking the momentum conservation of Ω^n without having an explicit source term, i.e. $S_i = 0$. This is done via a shift in the velocity used for computing the equilibrium distribution f_i^{eq} (cf. Eq. (8)). The new

equilibrium velocity is described by

$$[\text{SC}] \quad (\rho \mathbf{u})^{\text{eq}n} = \sum_i f_i^n \mathbf{c}_i + \tau \mathbf{K}^{\text{BGK}}. \quad (28)$$

The force coincides with the first moment of Ω^{BGK} ,

$$\begin{aligned} \sum_i \Omega^{\text{BGK}}(f_i^{\text{BGK}}) c_{i\alpha} &= -\frac{1}{\tau} \left((\rho u_\alpha)^{\text{BGK}} - (\rho u_\alpha)^{\text{eq} \text{BGK}} \right) \\ &= \frac{1}{\tau} \left((\tau K_\alpha)^{\text{BGK}} \right) = \mathbf{K}^{\text{BGK}}. \end{aligned} \quad (29)$$

The equilibrium velocity for the non-GCD method is $\mathbf{v}^{\text{eq}} = (\sum_i f_i \mathbf{c}_i + \tau \mathbf{K})/\rho$. Following the same steps as before to find the BGK velocity \mathbf{u}^{BGK} (cf. Eq. (23)), it follows

$$[\text{SC}] \quad \mathbf{u}^{\text{eq} \text{BGK}} = \frac{1}{\rho^{\text{tot}}} \sum_i f_i \mathbf{c}_i + \frac{\tau}{\rho^{\text{tot}}} \mathbf{K}^{\text{tot}}. \quad (30)$$

Thus, in the framework of GCD, when using the SC forcing, it follows that $\mathbf{u}^{\text{eq} \text{BGK}} = \mathbf{v}^{\text{eq}}$. Hence, the SC forcing scheme can be used for partial bounceback without any modification – no prefactors are required.

In the following, Guo forcing in the context of partial bounceback methods is investigated. Here, S_i is the second order accurate implementation of the force term F_i . For BGK dynamics, F_i is defined as

$$[\text{Guo}] \quad F_i^n(\mathbf{K}^n, \mathbf{u}^n) = w_i \left(\frac{c_{i\alpha}}{c_s^2} + \frac{u_\beta^n (c_{i\alpha} c_{i\beta} - c_s^2 \delta_{\alpha\beta})}{c_s^4} \right) K_\alpha^n. \quad (31)$$

The second-order accuracy is ensured by formulating $S_i^{\text{BGK}} = (1 - 1/(2\tau))F_i^{\text{BGK}}$ to cancel out the $1/(2\tau)\mathbf{K}^{\text{BGK}}$ emerging from Ω^{BGK} . When using a non-BGK collision operator, the source term formulation may change.

The crux to recover the conventional forcing scheme lies in the velocity definition. For the non-GCD velocity with forces $\mathbf{v} = (\sum_i f_i \mathbf{c}_i + \mathbf{K}/2)/\rho$. In the GCD framework the velocity based on Eq. (5), with $\sum_i (\Omega^{\text{BGK}}(f_i^{\text{BGK}}) + S_i^{\text{BGK}}) \mathbf{c}_i = \mathbf{K}^{\text{BGK}}$ is

$$\mathbf{u}^{\text{BGK}} = \frac{1}{\rho^{\text{tot}}} \sum_i f_i \mathbf{c}_i + \frac{1}{2\rho^{\text{tot}}} \mathbf{K}. \quad (32)$$

Here, the η^{BGK} cancel out, resulting again in $\mathbf{u}^{\text{BGK}} = \mathbf{v}$. Therefore, Eq. (31) becomes

$$[\text{Guo}] \quad F_i^{\text{BGK}}(\mathbf{K}^{\text{BGK}}, \mathbf{u}^{\text{BGK}}) = \eta^{\text{BGK}} F_i^{\text{BGK}}(\mathbf{K}, \mathbf{v}). \quad (33)$$

Thus, when using the Guo forcing scheme for partial bounceback, the force term requires a prefactor.

The velocities used in the forcing schemes (\mathbf{u}^{BGK} and $\mathbf{u}^{\text{eq} \text{BGK}}$) are unchanged compared to their conventional counterparts. However, the total velocity is impacted,

$$\begin{aligned} (\rho \mathbf{u})^{\text{tot}} &= \sum_{i,n} f_i^n \mathbf{c}_i + \frac{1}{2} \sum_{i,n} [\Omega_i^n(f_i^n) + S_i^n] \mathbf{c}_i, \\ &= \sum_i f_i \mathbf{c}_i + \frac{1}{2} \left[-2\eta^{\text{BGK}} \sum_i f_i \mathbf{c}_i + \eta^{\text{BGK}} \mathbf{K}^{\text{tot}} \right]. \end{aligned} \quad (34)$$

This definition is commonly seen as the macroscopic velocity in literature, often argued as the average momentum pre- and post-collision [11, 8]. For the BGK terms, the $\Omega^{\text{BGK}}(f_i^{\text{BGK}})$ and S_i^{BGK} together result in \mathbf{K}^{BGK} when taking the first moment. Both forcing methods used here are equivalent up to second order in $|\mathbf{K}|$ and third order in $|\mathbf{u}|$ [2, 45].

The GCD framework shows more systematically where and why prefactors are required. This is particularly useful when GCD is used for multiprocess

phenomena such as multiphase flow in multiscale porous media [17, 48].

3.3. Analysis of advection-diffusion flux boundary conditions

The GCD framework can also be applied to existing dynamics, analyzing them using a combined bottom-up and top-down approach. Previously, a bottom-up approach was used, i.e. simple collision operators were combined to generate complex dynamics. The top down approach decomposes complex into simple collision operators. We show this procedure by analyzing a robin-type boundary condition (cf. Eq. (17)).

In its extremes of $k_i = 0$ or $k_i \rightarrow \infty$, the RBC recovers the BB and ABB collision operators, respectively. Using those as the basis for a composite dynamic gives ²

$$\Omega^{\text{RBC}}(f_i) = \Omega^{\text{ABB}}(f_i^{\text{ABB}}) + \Omega^{\text{BB}}(f_i^{\text{BB}}). \quad (36)$$

From the GCD framework the following relations hold, $\eta_i^{\text{BB}} + \eta_i^{\text{ABB}} = 1$ and $\rho_w^n = \eta_i^n \rho^{\text{tot}}$. The wall velocity is usually known and imposed $\mathbf{u}_w^n \neq (\sum_i f_i^n \mathbf{c}_i) / \rho^n$. Hence, Eq. (36) becomes

$$\Omega^{\text{RBC}}(f_i) = \eta_i^{\text{ABB}} \Omega^{\text{ABB}}(f_i) + \eta_i^{\text{BB}} \Omega^{\text{BB}}(f_i). \quad (37)$$

Then using the decomposed ES formulations (cf. Eq. (14))

²From another perspective, the RBC is a combination of a scalar Dirichlet and Neumann boundary conditions. The Dirichlet boundary condition is given by the ABB and the Neumann boundary condition is approximated by the BB.

³, allows for combining Eqs. (14) and (37) and writing the composite RBC as

$$\Omega^{\text{RBC}}(f_i) = 2\eta_i^{\text{ABB}} \Omega^{\text{ES}}(f_i) + (\eta_i^{\text{BB}} - \eta_i^{\text{ABB}}) \Omega^{\text{BB}}(f_i). \quad (38)$$

To relate this composite dynamic formulation of the RBC with the one from literature (cf. Eq. (17)), it needs to be rewritten. Realizing that the two fractions in the scheme always add to one, i.e. $(2k_i)/(1+k_i) + (1-k_i)/(1+k_i) = 1$, allows splitting the $-f_i^n$ term, and expressing the literature RBC (cf. Eq. (17)) as a composite dynamic

$$\Omega^{\text{RBC}}(f_i^n) = \frac{2k_i}{1+k_i} \Omega^{\text{ES}}(f_i^n) + \frac{1-k_i}{1+k_i} \Omega^{\text{BB}}(f_i^n). \quad (39)$$

Assuming that the RBC is the sole dynamic, equates $f_i^n = f_i$ in Eq. (39). Then comparing Eqs. (38) and (39) allows for the computation of the composite fractions in Eq. (37). They are $\eta_i^{\text{ABB}} = k_i/(1+k_i)$ and $\eta_i^{\text{BB}} = 1/(1+k_i)$. This follows the pattern observed for the partial bounceback methods (cf. Eq. (19)), as η_i^{BB} can be rewritten as

$$\eta_i^{\text{BB}} = \frac{1}{\tau(\mathbf{c}_i \cdot \mathbf{n})k_r/D + 1}, \quad (40)$$

while remaining dependent on \mathbf{c}_i , with the scalar diffusivity $D := c_s^2(\tau - 1/2)$. For a fluid, the viscosity is the momentum diffusivity. Hence it makes sense instead of viscosity the scalar diffusivity appears here. Here, the transfer rate k_r is then analogous to

³On a slight tangent, since the ES is a composite dynamic consisting of ABB and BB with equal proportions, the ES a special case of the RBC. Or, from the point of the ES, the RBC is an off-centric version of the ES.

the permeability k . The similarity of the η_i definitions indicates a general theme.

To conclude this part, using the GCD framework, the RBC was broken down into simpler, better understood collision operators. This allows for the following insights: 1) It straightforwardly shows how this RBC can be extended to include a wall velocity, by using the full BB and ABB equations Eqs. (9) and (12). 2) By replacing the BB and ABB with different, yet physically equivalent operators, such as NEBB or interpolated BB found in literature, new RBC dynamics are generated.

While the RBC for first order equilibrium reactions was used here as an example, it can be applied to other RBC presented in literature, e.g. in Ref. [43]. Furthermore, any other complex collision operator can be analyzed as such, e.g. the very similar thermal contact resistance in Ref. [14].

3.4. Partial robin boundary condition

In this subsection, the GCD is used to generate a new dynamics, the partial RBC (PRBC). It models a wall where a section has some transfer. This can be interpreted as a superimposition of a reactive and non-reactive wall. Reactions are used here for illustration purposes, but this is valid for mass or heat flows as well. The impact of this imposition is discussed near the end of this section.

The two dynamics being combined are the RBC, discussed in Section 3.3, and the BB method. The

resulting operator reads ⁴

$$\Omega^{\text{PRBC}}(f_i) = \Omega^{\text{RBC}}(f_i^{\text{RBC}}) + \Omega^{\text{BB}}(f_i^{\text{BB}}). \quad (41)$$

This dynamic can model sub-grid effects. For illustration, nucleation is used as a physical example. A nuclei's size is usually a just few nanometers, certainly much smaller than the grid size of the simulation. Hence, a grid point is better simulated as a partially reactive wall, where the majority of the surface is non-reactive.

In the following, a purely diffusion driven simulation is used to compare a fully resolved RBC and BB boundary versus the proposed PRBC. A visual representation is shown for one particular case in Fig. 1, with a domain of 50×200 . The Péclet number ($Pe = LU/D$) is 1, and lattice velocity is $U = 0.02$. The reaction is defined via the Damköhler number ($Da = k_r/U$) and k_r is varied. At the right boundary ($x = 50$), a density Dirichlet condition is set with $\rho = 1$, the domain in the y-axis is periodic. In our nucleation example, ρ is representing concentration. The left boundary ($x = 0$), either consists of 1) the proposed continuous PRBC or 2) an alternating fully reactive – fully BB boundary condition.

The number of fully BB grid points between each RBC grid point is N_{BB} and will be used in the computation of η^{PRBC} . An example simulation comparing

⁴Since the $\Omega^{\text{RBC}}(f_i^{\text{RBC}})$ is also a composite of the ABB and BB dynamics, the PRBC dynamics can also be written as

$$\Omega^{\text{PRBC}}(f_i) = \Omega^{\text{ABB}}(f_i^{\text{RBC}}) + \Omega^{\text{BB}}(f_i^{\text{BB}} + f_i^{\text{RBC}}).$$

Hence, the PRBC is a RBC with an effective transfer rate k_r^{eff} .

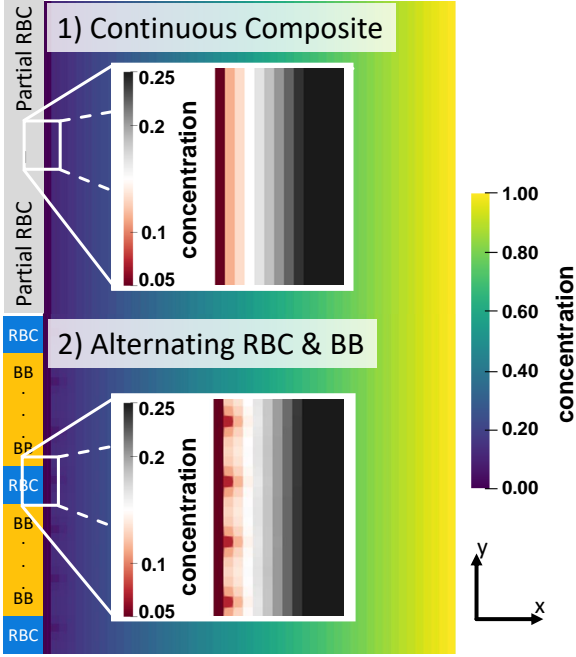


Figure 1: Steady-state simulation results comparing the novel PRBC to resolved BB-RBC setup. A spacing of $N_{BB} = 5$ with a $Da = 500$ is used. For the PRBC, the composite fraction used is $\eta^{RBC} = 1/9$. The inset shows a zoom near the wall to highlight the effects in that region.

the two methods is given in Fig. 1, where the top half is the novel PRBC and the bottom half alternating fully reactive.

The comparison in Fig. 1 shows a spacing of $N_{BB} = 5$ with a $Da = 500$ and corresponding $\eta^{RBC} = 1/9$ to match the alternating case. Other Damköhler numbers, spacing, and η^{RBC} values were also simulated and plotted in Fig. 2. For these simulations, the composite fraction is given by

$$\eta^{RBC} = \frac{1}{AN_{BB} + 1}. \quad (42)$$

Here, A is a parameter to fit the composite to the resolved simulation result. Defining the composite fraction that way continues the trend of the previous

methods (cf. Eq. (19) and Eq. (40)). Since only one reactive grid point is simulated $N_{RBC} = 1$, the impact of multiple reactive grid points are not shown. However logically, the relevant factor is N_{BB}/N_{RBC} . This is true especially for the reaction limited case ($PeDa \ll 1$), where the exact location of the reactive grid points are negligible.

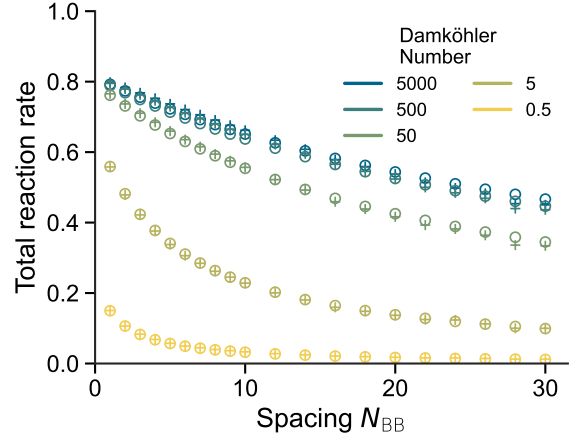


Figure 2: Comparison of non-dimensional reaction rates from boundary condition using the alternating (pluses) vs PRBC (circles). The spacing N_{BB} is varied between 1 and 30. The Damköhler numbers $Da = \{0.5, 5, 50, 500, 5000\}$ were simulated, where the fitting parameter $A = \{1, 1, 1.3, 1.9, 2.0\}$ were used, respectively.

Due the wall length being a fixed 200 grid points, certain N_{BB} spacings have the same number of fully reactive grid points. For example $N_{BB} = \{22, 24\}$, and $N_{BB} = \{28, 30\}$ have 9 and 7 reactive grid points, respectively. However, for the higher spacing of each of the two pairs, the distribution is slightly worse, hence decreasing the diffusion towards the reactive grid points and thus slightly decreasing total reactions, as can be seen in Fig. 2.

From Fig. 2, it is clear that the relation of Eq. (42)

captures the behavior, as long as an appropriate value for A is used. A sensitivity analysis of A is given in Appendix C.

The parameter A is related to how reaction- or diffusion-limited the system is, with reaction limit $A = 1$ and diffusion limit $A \rightarrow A_{\text{lim}}$. The A_{lim} is a constant related to the system geometry at hand, which in our case is approximately 2.

That is a consequence of the imposition. This assumes that the time scale within the grid point is very fast, and thus negligible. That results in an effectively infinitely fast diffusion within the PRBC grid point. In case the setup is diffusion limited, the time scale becomes relevant, which can be represented as if there are effectively fewer N_{RBC} or more N_{BB} .

Overall, this new PRBC can find applications where the boundary behavior is driven by a different length scale used in the bulk. Such as nuclei or nano-particles on substrates for reactions, injectors for mass fluxes in large chambers, or conductive fibers in non-conductive resin.

3.5. Semi-permeable advection-diffusion with transfer

In this showcase, a semi-permeable advection-diffusion with transfer dynamics is shown. The transfer can be density, temperature, or concentration, depending on what is simulated. It combines fluid flow and the robin boundary condition, using BGK and RBC. Macroscopically, that results in a mixture of flow, wall and fluxes. In GCD formulation, they give a transfer partial bounceback (TPBB) composite dy-

namics described by the collision operator ⁵

$$\Omega^{\text{TPBB}}(f_i) = \Omega^{\text{RBC}}(f_i^{\text{RBC}}) + \Omega^{\text{BGK}}(f_i^{\text{BGK}}). \quad (43)$$

For illustration sticking with reactions, this represents advection-diffusion through a reactive porous media. For particulate mass flow, this could be a dust filter for example.

In the limit of no transfer, $k_r = 0$ (cf. Eq. (40)), the RBC recovers BB dynamics, thus the TPBB results in the known partial-bounceback BGK-BB method. For all transfer coefficients $k_r > 0$, it would be a new dynamic.

Intuitively, we can assume that a mixture of flow, wall and fluxes should result in some kind of semi-permeable PBB dynamics with transfer. In Appendix D, we show that it is indeed the case, with TPBB able to be rewritten into

$$\Omega^{\text{TPBB}}(f_i) = \Omega^{\text{PBB}}(f_i) - 2\eta^{\text{RBC}}\eta^{\text{ABB}}f_i^{\text{neq}}. \quad (44)$$

In this rewritten form, the TPBB clearly shows the advection-diffusion through porous media, with $\Omega^{\text{PBB}}(f_i) = \Omega^{\text{BGK}}(f_i^{\text{BGK}}) + \Omega^{\text{BB}}(f_i^{\text{RBC}})$, and has a source term of $-2\eta^{\text{RBC}}\eta^{\text{ABB}}f_i^{\text{neq}}$, where $f_i^{\text{neq}} = f_i - f_i^{\text{eq}}$. The $\Omega^{\text{PBB}}(f_i)$ simulates diffusion with an effective lower diffusivity due to tortuosity [11]. The source term $f_i^{\text{neq}} \sim (\rho^{\text{eq}} - \rho)$ is related to the density difference, but accounts for the advective flux. It vanishes as the density difference approaches the equilibrium density. The η^{RBC} already contains τ dependent corrective terms.

⁵Since Ω^{RBC} is itself a composite dynamic, the TPBB is a composite of three different collision operators.

This new dynamic is showcased here as a reactive membrane in a quasi-1D reaction-diffusion problem. Simulated is a 2D domain of size 10×50 , periodic in the y -axis, with two Dirichlet boundaries defining the concentration to $\rho = 0$ at $x = 0$ and $\rho = 1$ at $x = 50$. A semi-permeable membrane is initialized from $x = 16$ to $x = 33$. The equilibrium concentration is $\rho^{\text{eq}} = 0$, it is defined that $\mathbf{c}_i \cdot \mathbf{n} = 1$ for all i , the relaxation time is $\tau = 0.8$. A variation in the Damköhler number and composite fraction η^{RBC} is performed. The resulting concentration profile are shown in Figs. 3 and 4.

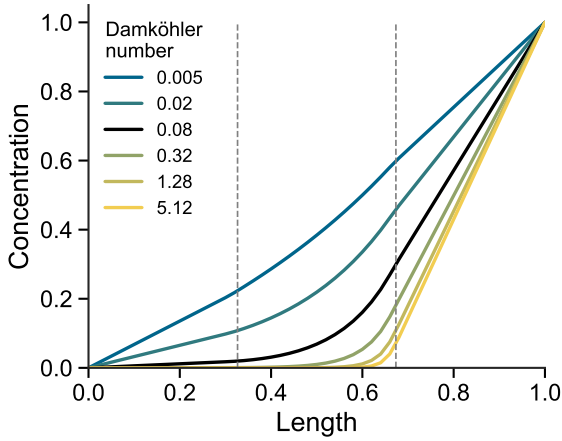


Figure 3: Simulation results of semi-permeable diffusion with a reactive membrane in between the dashed lines. The impact of variations of the reaction rate is shown. The black line is the common baseline. The composite fraction $\eta^{\text{RBC}} = 0.1$.

From the concentration profiles seen in Figs. 3 and 4, there are three distinct regions: the membrane indicated by the dashed box, and the two freely diffusive regions to the left and right of the membrane. In the freely diffusive regions, the concentration profile is linear, as one would expect. Inside the membrane, the concentration profile is increasing exponentially.

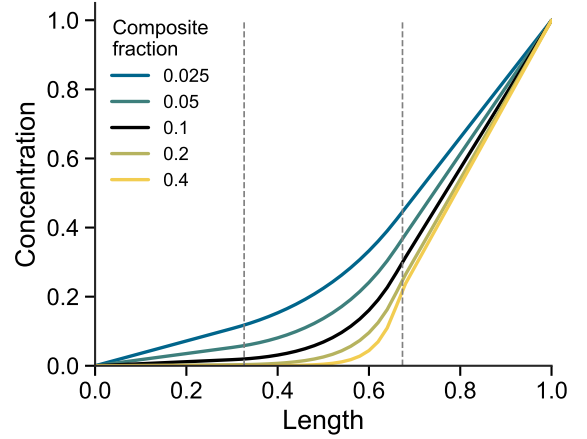


Figure 4: Simulation results of semi-permeable diffusion with a reactive membrane in between the dashed lines. The impact of variations of the composite fractions η^{RBC} are shown. The black line is the common baseline. The reaction rate is constant at $\text{Da} = 0.08$.

Both the Damköhler number and the composite fraction impact exponentiality and the reactivity of the membrane. However, the exponentiality is mostly determined by the composite fraction η^{RBC} (cf. Fig. 4). However, the Damköhler number has a larger impact on the concentration decrease than the composite fraction.

Since for advection-diffusion, the composite fraction is related to the tortuosity of the medium [11], this type of dynamics can simulate the impact of a change in the tortuosity. This can be applied to study various systems, e.g. particles flowing through filters, precipitation in nano-porous battery electrodes, or heat flow through a radiator.

4. Concluding remarks

We proposed a generalized framework for composite dynamics within the lattice Boltzmann method. This framework decomposes the total populations into population parts, applying a specific collision operator to each, before finally recombining them. This enables modeling of complex physical phenomena through combination of various simple collision operators.

The validity of the GCD framework is demonstrated by recovering the same equations as the partial bounceback methods for semi-permeable fluid flow in existing literature. In contrast to them, the framework provides mathematical reasoning for the incorporation of forces, thus addressing a gap in the current literature.

Furthermore, it is shown how using this GCD approach may serve as a valuable analysis method. Exemplary, it is shown that a flux boundary condition can be represented as a composition of bounceback and anti-bounceback dynamics. The generality allows for the analysis of arbitrarily complex dynamics.

The potential of the GCD framework has yet to be fully explored. Several research avenues remain open. One possibility is to investigate the trend in composite fraction and macroscopic behavior. Another is to account for inter-dynamics interaction. Also of interest is extending the current models to anisotropic composite fractions. And finally, investigating the GCD framework's applicability and limits for non-local dynamics. Overall, the framework provides a system-

atic approach to derive lattice Boltzmann methods for complex physical processes.

Acknowledgments

The authors gratefully acknowledge financial support by the Federal Ministry of Education and Research (BMBF) within the project "SulForFlight" under the Grant No.03XP0491A. M.L. and B.K. gratefully acknowledge financial support from the European Union's Horizon 2020 Research and Innovation Programme within the project "DEFACTO" under the grant number 875247. This work contributes to the research performed at CELEST (Center for Electrochemical Energy Storage Ulm-Karlsruhe).

Author Declarations

Conflict of Interest

The authors have no conflicts to disclose.

Author Contributions

Julius Weinmiller: Conceptualization; Investigation; Methodology; Software; Visualization; Writing – original draft; **Benjamin Kellers:** Conceptualization; Methodology; Validation; Writing – review & editing; **Martin P. Lautenschlaeger:** Conceptualization; Writing – review & editing; **Timo Danner:** Conceptualization; Funding acquisition; Project administration; Supervision; Writing – review & editing; **Arnulf Latz:** Funding acquisition; Supervision; Writing – review & editing;

Data Availability Statement

Data sharing is not applicable to this article as no new data were created or analyzed in this study.

Appendix A. Subtracting BB from ABB calculations

In this section, we will show the result of the subtraction of the BB collision operator from the ABB collision operator. Inserting the definitions of the collision operators results in

$$\begin{aligned} \Omega^{\text{ABB}}(f_i) - \Omega^{\text{BB}}(f_i) = & \\ & \left(-f_i - f_{\bar{i}} + 2w_i\rho_w \left(1 + \frac{u_{w\alpha}u_{w\beta} (c_{i\alpha}c_{i\beta} - c_s^2\delta_{\alpha\beta})}{2c_s^4} \right) \right) \\ & - \left(-f_i + f_{\bar{i}} + 2w_i\rho_w \frac{c_{i\alpha}u_{w\alpha}}{c_s^2} \right). \end{aligned}$$

Canceling out $-f_i$, and collecting $f_{\bar{i}}$ and like terms results in

$$\begin{aligned} \Omega^{\text{ABB}}(f_i) - \Omega^{\text{BB}}(f_i) = & \\ & -2f_{\bar{i}} + 2w_i\rho_w \left(1 - \frac{c_{i\alpha}u_{w\alpha}}{c_s^2} \right. \\ & \left. + \frac{u_{w\alpha}u_{w\beta} (c_{i\alpha}c_{i\beta} - c_s^2\delta_{\alpha\beta})}{2c_s^4} \right). \end{aligned}$$

The second term looks suspiciously similar to $2 \times f_i^{\text{eq}}$, twice the equilibrium function (cf. Eq. (8)). However, the $\frac{c_{i\alpha}u_{w\alpha}}{c_s^2}$ term is here negative, not positive. But we are looking at it from the wrong direction. Instead of i , we need to look at \bar{i} . Then $c_{\bar{i}\alpha} = -c_{i\alpha}$ and $w_i = w_{\bar{i}}$. For the terms of even velocity order (u^0 and u^2) the negative cancel out, negating only the odd terms.

With that, the final expression is

$$\begin{aligned} \Omega^{\text{ABB}}(f_i) - \Omega^{\text{BB}}(f_i) = & \\ & -2f_{\bar{i}} + 2w_i\rho_w \left(1 + \frac{c_{\bar{i}\alpha}u_{w\alpha}}{c_s^2} \right. \\ & \left. + \frac{u_{w\alpha}u_{w\beta} (c_{\bar{i}\alpha}c_{\bar{i}\beta} - c_s^2\delta_{\alpha\beta})}{2c_s^4} \right), \end{aligned}$$

finally ending in

$$\Omega^{\text{ABB}}(f_i) - \Omega^{\text{BB}}(f_i) = -2f_{\bar{i}} + 2f_{\bar{i}}^{\text{eq}} = -2f_{\bar{i}}^{\text{neq}}.$$

To summarize:

$$\frac{\Omega^{\text{ABB}}(f_i) - \Omega^{\text{BB}}(f_i)}{2} = -f_{\bar{i}}^{\text{neq}} \quad (\text{A.1})$$

Appendix B. Comparison Partial Bounceback

This section appendix contains a more complete comparison of the PBB found in literature. Here, we need to look at the PBB equation with an additional term for any remaining collision terms

$$f_i^* = f_i + \Omega^{\text{BGK}}(f_i^{\text{BGK}}) + \Omega^{*\text{BB}}(f_i^{*\text{BB}}) + \sum_n \Omega^n(f_i^n). \quad (\text{B.1})$$

Note that for a pure no-slip walls and fluid flow composite dynamics, $\sum_n \Omega^n(f_i^n) = 0$. There are a few methods for which that is not the case shown in Table B.1.

The ‘‘fullway collision’’ and ‘‘preemptive’’ methods have this additional term. Lets interpret the third collision operator as a ‘‘Reversed BGK’’ (RBGK), $\Omega^{\text{RBGK}}(f_i^{\text{RBGK}})$, with $\eta^{\text{RBGK}} = \eta^{*\text{BB}} > 0$. Then either 1) it is a collision term and then the total population, by definition the sum of all the composite fractions, is $\sum_n \eta^n = 1 + \eta^{*\text{BB}} > 1$ and these methods

Table B.1: Overview of collision operators and GCD composite fractions used in partial bounceback methods.

Bounceback method	$\Omega^{*BB}(f_i^{*BB}) =$	$\sum_n \Omega^n(f_i^n) =$	$\eta^{*BB} =$
Fullway [11]	$\Omega^{BB}(f_i^{*BB})$	0	$\frac{1}{2k/v+1}$
Fullway collision [7, 9]	$\Omega^{BB}(f_i^{*BB})$	$-\frac{1}{\tau} \left(f_i^{*BB} - f_i^{eq}(\rho^{*BB}, \mathbf{u}^{BGK}) \right)$	$\frac{1}{2k/v+2}$
Preemptive ^a [5]	$-f_i^{*BB} + \tilde{f}_i^{*BB}$	$-\frac{1}{\tau} \left(\tilde{f}_i^{*BB} - \tilde{f}_i^{eq}(\tilde{\rho}^{*BB}, \tilde{\mathbf{u}}^{BGK}) \right)$	$\frac{1}{2k/v}$
Quasi-halfway ^b [6]			$\frac{1}{2k/v+1}$
Non-equilibrium [4]	$\Omega^{NEBB}(f_i^{*BB})$	0	$\frac{1}{c_s^2(1+\bar{\varepsilon})/v+\bar{\varepsilon}}$ ^c

^a A non-local method. Here $\tilde{\square}$ refers to properties at $\mathbf{x} + \mathbf{c}_i$.

^b A PBB which modifies the streaming step and not the collision.

^c Here, $\bar{\varepsilon}$ is a smoothing factor equivalent to $1/\varepsilon$ in Ref. [4].

do not follow the GCD, or 2) the $\Omega^{RBGK}(f_i^{RBGK})$ is a source term that neither impacts density nor momentum, but some other mesoscopic terms.

Appendix C. PRBC paramter A sensitivity

In the PRBC, the composite fraction η^{RBC} is dependent on a fitting parameter A (cf. Eq. (42)). Here, the sensitivity of this parameter is shown for one simulation. The $Da = 50$ simulation is used, since it is neither diffusion, nor reaction limited, and thus should be most sensitive to variation of A . The results are shown in Fig. C.1.

From Fig. C.1, it can be concluded that the fitting parameter has the largest impact when the spacing is very large. For small spacing, the impact is negligible. Even for the worst case with large spacing, the simulation is more sensitive to a decrease in the reaction rate, than to a variation in the fitting parameter.

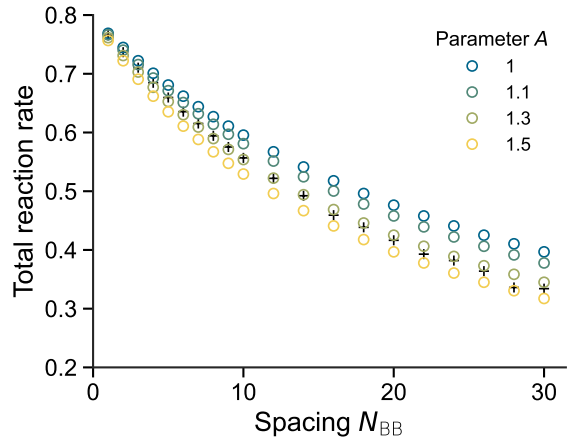


Figure C.1: Sensitivity of the fitting parameter A on simulated non-dimensional reaction rate. The reaction rates of the boundary condition using the alternating BC (black pluses) vs PRBC (colored circles) are shown. The spacing N_{BB} is varied between 1 and 30. The Damköhler number $Da = 50$ was simulated with fitting parameters $A = \{1, 1.1, 1.3, 1.5\}$.

Appendix D. Rewriting the TPBB collision operator

In this section, we will show the mathematical steps to get from the original TPBB formulation (cf. Eq. (43)) to the PBB with a source formulation (cf. Eq. (44)).

Since Ω^{RBC} is itself a composite dynamic, the TPBB is a composite of three different collision operators; BGK, ABB and BB. The composite fractions are η^{BGK} , $\eta^{\text{RBC}}\eta^{\text{ABB}}$ and $\eta^{\text{RBC}}\eta^{\text{BB}}$, respectively, where $\eta^{\text{BGK}} + \eta^{\text{RBC}} = 1$ and $\eta^{\text{ABB}} + \eta^{\text{BB}} = 1$.

Starting with the original formulation Eq. (43)

$$\Omega^{\text{TPBB}}(f_i) = \Omega^{\text{RBC}}(f_i^{\text{RBC}}) + \Omega^{\text{BGK}}(f_i^{\text{BGK}}),$$

the first step is to take out the composite fractions

$$\Omega^{\text{TPBB}}(f_i) = \eta^{\text{RBC}}\Omega^{\text{RBC}}(f_i) + \eta^{\text{BGK}}\Omega^{\text{BGK}}(f_i).$$

Then we expand the Ω^{RBC} to the ABB and BB components

$$\begin{aligned} \Omega^{\text{TPBB}}(f_i) = & \eta^{\text{RBC}} [\Omega^{\text{ABB}}(f_i^{\text{ABB}}) + \Omega^{\text{BB}}(f_i^{\text{BB}})] \\ & + \eta^{\text{BGK}}\Omega^{\text{BGK}}(f_i). \end{aligned}$$

We again take out the composite fractions, and then express the $\eta^{\text{BB}} = 1 - \eta^{\text{ABB}}$, resulting in

$$\begin{aligned} \Omega^{\text{TPBB}}(f_i) = & \eta^{\text{RBC}} [\eta^{\text{ABB}}\Omega^{\text{ABB}}(f_i) + (1 - \eta^{\text{ABB}})\Omega^{\text{BB}}(f_i)] \\ & + \eta^{\text{BGK}}\Omega^{\text{BGK}}(f_i). \end{aligned}$$

Collecting the $\eta^{\text{BGK}}\Omega^{\text{BGK}}$ and $\eta^{\text{RBC}}\Omega^{\text{BB}}$ as a PBB collision operator as here $\eta^{\text{RBC}} + \eta^{\text{BGK}} = 1$

$$\Omega^{\text{PBB}}(f_i) = \eta^{\text{BGK}}\Omega^{\text{BGK}}(f_i) + \eta^{\text{RBC}}\Omega^{\text{BB}},$$

results in the simplification

$$\begin{aligned} \Omega^{\text{TPBB}}(f_i) = & \eta^{\text{RBC}}\eta^{\text{ABB}} [\Omega^{\text{ABB}}(f_i) - \Omega^{\text{BB}}(f_i)] \\ & + \Omega^{\text{PBB}}(f_i). \end{aligned}$$

From Appendix A we know that

$$\frac{\Omega^{\text{ABB}}(f_i) - \Omega^{\text{BB}}(f_i)}{2} = -f_i^{\text{neq}},$$

hence the final form is

$$\Omega^{\text{TPBB}}(f_i) = -2\eta^{\text{RBC}}\eta^{\text{ABB}}f_i^{\text{neq}} + \Omega^{\text{PBB}}(f_i). \quad (\text{D.1})$$

References

- [1] R. Benzi, S. Succi, M. Vergassola, The lattice Boltzmann equation: Theory and applications, *Physics Reports* 222 (3) (1992) 145–197. doi:10.1016/0370-1573(92)90090-M.
- [2] T. Krüger, H. Kusumaatmaja, A. Kuzmin, O. Shardt, G. Silva, E. M. Viggen, *The Lattice Boltzmann Method: Principles and Practice*, Graduate Texts in Physics, Springer International Publishing, Cham, 2017. doi:10.1007/978-3-319-44649-3.
- [3] O. Dardis, J. McCloskey, Lattice Boltzmann scheme with real numbered solid density for the simulation of flow in porous media, *Physical Review E* 57 (4) (1998) 4834–4837. doi:10.1103/PhysRevE.57.4834.
- [4] D. R. Noble, J. R. Torczynski, A Lattice-Boltzmann Method for Partially Saturated Computational Cells, *International Journal of Modern Physics C* 09 (08) (1998) 1189–1201. doi:10.1142/S0129183198001084.
- [5] D. Thorne, M. Sukop, Lattice Boltzmann model for the elder problem, in: *Developments in Water Science*, Vol. 55, Elsevier, 2004, pp. 1549–1557. doi:10.1016/S0167-5648(04)80165-5.
- [6] H. Yoshida, H. Hayashi, Transmission–Reflection Coefficient in the Lattice Boltzmann Method, *Journal of Statistical Physics* 155 (2) (2014) 277–299. doi:10.1007/s10955-014-0953-7.
- [7] J. Zhu, J. Ma, An improved gray lattice Boltzmann model for simulating fluid flow in multi-scale porous media, *Advances in Water Resources* 56 (2013) 61–76. doi:10.1016/j.advwatres.2013.03.001.
- [8] I. Ginzburg, Comment on “An improved gray Lattice Boltzmann model for simulating fluid flow in multi-scale porous media”: Intrinsic links between LBE Brinkman schemes, *Advances in Water Resources* 88 (2016) 241–249. doi:10.1016/j.advwatres.2014.05.007.
- [9] J. Zhu, J. Ma, Extending a Gray Lattice Boltzmann Model for Simulating Fluid Flow in Multi-Scale Porous Media,

- Scientific Reports 8 (1) (2018) 5826. doi:10.1038/s41598-018-24151-2.
- [10] H. Yu, X. Chen, Z. Wang, D. Deep, E. Lima, Y. Zhao, S. D. Teague, Mass-conserved volumetric lattice Boltzmann method for complex flows with willfully moving boundaries, *Physical Review E* 89 (6) (2014) 063304. doi:10.1103/PhysRevE.89.063304.
- [11] S. D. Walsh, H. Burwinkle, M. O. Saar, A new partial-bounceback lattice-Boltzmann method for fluid flow through heterogeneous media, *Computers & Geosciences* 35 (6) (2009) 1186–1193. doi:10.1016/j.cageo.2008.05.004.
- [12] K. Han, Y. Feng, D. Owen, Modelling of thermal contact resistance within the framework of the thermal lattice Boltzmann method, *International Journal of Thermal Sciences* 47 (10) (2008) 1276–1283. doi:10.1016/j.ijthermalsci.2007.11.007.
- [13] W.-Z. Fang, H. Zhang, L. Chen, W.-Q. Tao, Numerical predictions of thermal conductivities for the silica aerogel and its composites, *Applied Thermal Engineering* 115 (2017) 1277–1286. doi:10.1016/j.applthermaleng.2016.10.184.
- [14] X. Li, D. Gao, B. Hou, X. Wang, An inserted layer LBM for thermal conduction with contact resistances, *Chemical Engineering Science* 233 (2021) 116431. doi:10.1016/j.ces.2020.116431.
- [15] C. Xie, J. Wang, D. Wang, N. Pan, M. Wang, Lattice Boltzmann Modeling of Thermal Conduction in Composites with Thermal Contact Resistance, *Communications in Computational Physics* 17 (4) (2015) 1037–1055. doi:10.4208/cicp.2014.m360.
- [16] G. G. Pereira, Grayscale lattice Boltzmann model for multiphase heterogeneous flow through porous media, *Physical Review E* 93 (6) (2016) 063301. doi:10.1103/PhysRevE.93.063301.
- [17] M. P. Lautenschlaeger, J. Weinmiller, B. Kellers, T. Danner, A. Latz, Homogenized lattice Boltzmann model for simulating multi-phase flows in heterogeneous porous media, *Advances in Water Resources* 170 (2022) 104320. doi:10.1016/j.advwatres.2022.104320.
- [18] A. Mink, K. Schediwy, C. Posten, H. Nirschl, S. Simonis, M. J. Krause, Comprehensive Computational Model for Coupled Fluid Flow, Mass Transfer, and Light Supply in Tubular Photobioreactors Equipped with Glass Sponges, *Energies* 15 (20) (2022) 7671. doi:10.3390/en15207671.
- [19] V. Aho, K. Mattila, T. Kühn, P. Kekäläinen, O. Pulkkinen, R. B. Minussi, M. Vihinen-Ranta, J. Timonen, Diffusion through thin membranes: Modeling across scales, *Physical Review E* 93 (4) (2016) 043309. doi:10.1103/PhysRevE.93.043309.
- [20] F. Verhaeghe, S. Arnout, B. Blanpain, P. Wollants, Lattice-Boltzmann modeling of dissolution phenomena, *Physical Review E* 73 (3) (2006) 1–10. doi:10.1103/PhysRevE.73.036316.
- [21] R. A. Patel, Lattice Boltzmann Method Based Framework for Simulating Physico-Chemical Processes in Heterogeneous Porous Media and Its Application to Cement Paste, Ph.D. thesis, Ghent University (2016).
- [22] L. Ju, C. Zhang, Z. Guo, Local reactive boundary scheme for irregular geometries in lattice Boltzmann method, *International Journal of Heat and Mass Transfer* 150 (2020) 119314. doi:10.1016/j.ijheatmasstransfer.2020.119314.
- [23] J. Weinmiller, M. P. Lautenschlaeger, B. Kellers, T. Danner, A. Latz, General Local Reactive Boundary Condition for Dissolution and Precipitation Using the Lattice Boltzmann Method, *Water Resources Research* 60 (2) (2024) e2023WR034770. doi:10.1029/2023WR034770.
- [24] Y. Gao, W. Zhou, Z. Wen, R. Dou, X. Liu, Meso-scale simulation of Li–O₂ battery discharge process by an improved lattice Boltzmann method, *Electrochimica Acta* 442 (2023) 141880. doi:10.1016/j.electacta.2023.141880.
- [25] M. P. Lautenschlaeger, B. Prifling, B. Kellers, J. Weinmiller, T. Danner, V. Schmidt, A. Latz, Understanding Electrolyte Filling of Lithium-Ion Battery Electrodes on

- the Pore Scale Using the Lattice Boltzmann Method, *Batteries & Supercaps* 5 (7) (Jul. 2022). doi:10.1002/batt.202200090.
- [26] G. Wang, U. D’Ortona, P. Guichardon, Improved partially saturated method for the lattice Boltzmann pseudopotential multicomponent flows, *Physical Review E* 107 (3) (2023) 035301. doi:10.1103/PhysRevE.107.035301.
- [27] L. Vienne, S. Marie, F. Grasso, Simulation of Viscous Fingering Instability by the Lattice Boltzmann Method, in: *AIAA Aviation 2019 Forum*, American Institute of Aeronautics and Astronautics, Dallas, Texas, 2019. doi:10.2514/6.2019-3432.
- [28] Z. Tian, J. Wang, Lattice Boltzmann simulation of CO₂ reactive transport in network fractured media: LBM CO₂ REACTIVE TRANSPORT, *Water Resources Research* 53 (8) (2017) 7366–7381. doi:10.1002/2017WR021063.
- [29] Z. Sun, Y. Yin, Y. Wu, Z. Sun, L. Zhu, Y. Zhan, V. Niasar, S. An, Morphological and hydrodynamic properties of hydrates during dissociation in sediment, *Fuel* 353 (2023) 129032. doi:10.1016/j.fuel.2023.129032.
- [30] P. Eibl, S. Rustige, C. Witz, J. Khinast, LBM for two-phase (bio-)reactors, in: *Advances in Chemical Engineering*, Vol. 55, Elsevier, 2020, pp. 219–285. doi:10.1016/b.s.ache.2020.04.003.
- [31] R. Petkantchin, A. Rousseau, O. Eker, K. Zouaoui Boudjeltia, F. Raynaud, B. Chopard, the INSIST investigators, A simplified mesoscale 3D model for characterizing fibrinolysis under flow conditions, *Scientific Reports* 13 (1) (2023) 13681. doi:10.1038/s41598-023-40973-1.
- [32] M. Gaedtker, S. Abishek, R. Mead-Hunter, A. J. C. King, B. J. Mullins, H. Nirschl, M. J. Krause, Total enthalpy-based lattice Boltzmann simulations of melting in paraffin/metal foam composite phase change materials, *International Journal of Heat and Mass Transfer* 155 (2020) 119870. doi:10.1016/j.ijheatmasstransfer.2020.119870.
- [33] H. Li, H. Wei, T. P. Padera, J. W. Baish, L. L. Munn, Computational simulations of the effects of gravity on lymphatic transport, *PNAS Nexus* 1 (5) (2022) pgac237. doi:10.1093/pnasnexus/pgac237.
- [34] S. An, H. Erfani, H. Hellevang, V. Niasar, Lattice-Boltzmann simulation of dissolution of carbonate rock during CO₂-saturated brine injection, *Chemical Engineering Journal* (October) (2020). doi:10.1016/j.cej.2020.127235.
- [35] P. L. Bhatnagar, E. P. Gross, M. Krook, A Model for Collision Processes in Gases. I. Small Amplitude Processes in Charged and Neutral One-Component Systems, *Physical Review* 94 (3) (1954) 511–525. doi:10.1103/PhysRev.94.511.
- [36] I. Ginzbourg, D. d’Humières, Local second-order boundary methods for lattice Boltzmann models, *Journal of Statistical Physics* 84 (5-6) (1996) 927–971. doi:10.1007/BF02174124.
- [37] A. J. C. Ladd, Numerical simulations of particulate suspensions via a discretized Boltzmann equation. Part 1. Theoretical foundation, *Journal of Fluid Mechanics* 271 (1994) 285–309. doi:10.1017/S0022112094001771.
- [38] I. Ginzburg, F. Verhaeghe, D. D’Humières, Two-relaxation-time Lattice Boltzmann scheme: About parametrization, velocity, pressure and mixed boundary conditions, *Communications in Computational Physics* 3 (2) (2008) 427–478.
- [39] I. Ginzburg, F. Verhaeghe, D. D’Humières, Study of simple hydrodynamic solutions with the two-relaxation-times lattice Boltzmann scheme, *Communications in Computational Physics* 3 (3) (2008) 519–581.
- [40] S. Izquierdo, N. Fueyo, Characteristic nonreflecting boundary conditions for open boundaries in lattice Boltzmann methods, *Physical Review E* 78 (4) (2008) 046707. doi:10.1103/PhysRevE.78.046707.
- [41] J. Latt, B. Chopard, O. Malaspinas, M. Deville, A. Michler, Straight velocity boundaries in the lattice Boltzmann method, *Physical Review E* 77 (5) (2008) 056703. doi:10.1103/PhysRevE.77.056703.
- [42] X. He, Q. Zou, L.-S. Luo, M. Dembo, Analytic solu-

tions of simple flows and analysis of nonslip boundary conditions for the lattice Boltzmann BGK model, *Journal of Statistical Physics* 87 (1-2) (1997) 115–136. doi:10.1007/BF02181482.

- [43] J. Huang, W.-A. Yong, Boundary conditions of the lattice Boltzmann method for convection–diffusion equations, *Journal of Computational Physics* 300 (2015) 70–91. doi:10.1016/j.jcp.2015.07.045.
- [44] G. Silva, I. Ginzburg, The permeability and quality of velocity field in a square array of solid and permeable cylindrical obstacles with the TRT–LBM and FEM Brinkman schemes, *Comptes Rendus. Mécanique* 343 (10-11) (2015) 545–558. doi:10.1016/j.crme.2015.05.003.
- [45] B. Postma, G. Silva, Force methods for the two-relaxation-times lattice Boltzmann, *Physical Review E* 102 (6) (2020) 063307. doi:10.1103/PhysRevE.102.063307.
- [46] Z. Guo, C. Zheng, B. Shi, Discrete lattice effects on the forcing term in the lattice Boltzmann method, *Physical Review E* 65 (4) (2002) 046308. doi:10.1103/PhysRevE.65.046308.
- [47] X. Shan, H. Chen, Lattice Boltzmann model for simulating flows with multiple phases and components, *Physical Review E* 47 (3) (1993) 1815–1819. doi:10.1103/PhysRevE.47.1815.
- [48] G. Pereira, Fluid flow, relative permeabilities and capillary pressure curves through heterogeneous porous media, *Applied Mathematical Modelling* 75 (2019) 481–493. doi:10.1016/j.apm.2019.05.050.